Supporting Information

Engineering Graphene Quantum Dots for Enhanced Ultraviolet and Visible Light p-Si Nanowire based Photodetector

Iuliana Mihalache[1*], Antonio Radoi[1], Razvan Pascu[1], Cosmin Romanitan[1,2], Eugenia Vasile[1,3], Mihaela Kusko[1*]

[1] National Institute for Research and Development in Microtechnologies (IMT Bucharest), 126A Erou Iancu Nicolae Street, 72996, Bucharest, Romania

[2] Faculty of Applied Chemistry and Material Science, University Politehnica of Bucharest, No. 1-7 Gh. Polizu Street, 011061 Bucharest, Romania

[3] Faculty of Physics, University of Bucharest, P.O. Box MG-11, 077125 Bucharest, Romania

Corresponding authors:

*E-mail: iuliana.mihalache@imt.ro; mihaela.kusko@imt.ro;

Figure S1 – Cyclic voltammograms of self-passivated GQDs, and PEI modified GQDs.

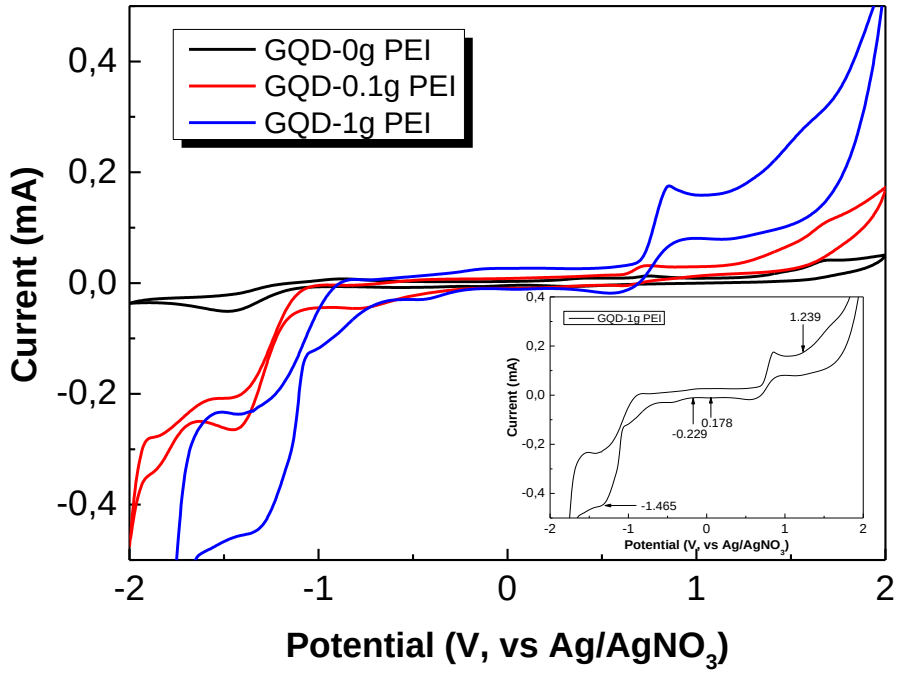

The onset - potentials of the oxidation and reduction peaks related to electron and hole injection into the conduction and valence bands were used to determine the E_{HOMO} (from $E_{ox,\ onset}$) and E_{LUMO} (from $E_{red,\ onset}$) using the following two equations:

$$E_{HOMO} = -e\left(4.75 + E_{ox,onset}\right)(eV) = -6.02\ eV \qquad (1)$$

$$E_{LUMO} = -e\left(4.75 + E_{red,onset}\right)(eV) = -3.28\ eV \qquad (2)$$

Figure S2 – X-ray diffraction patterns of the bulk Si, SiNWs and GQD^{PEI} coated SiNWs.

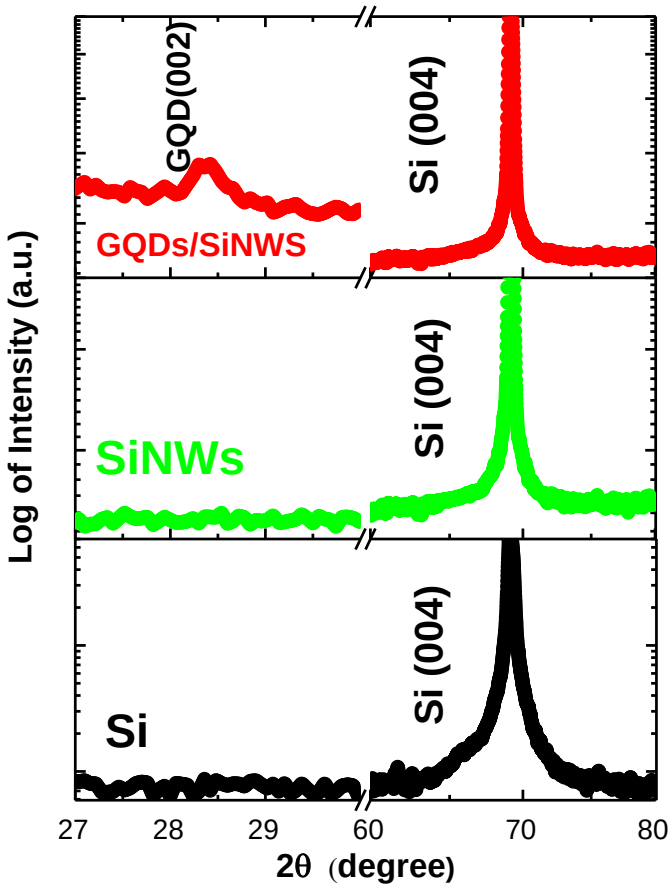

Figure S3 – Optimization steps based on photodetection performance analysis:

(a) *SiNWs length test* - heterostructures fabricated by loading 4 types SiNWs substrates with 1, 2, and 3 layers of GQD^{PEI}s;

(b) *GQD^{PEI}s concentration test* – heterostructures fabricated by loading on SiNWs substrates 1 layer of GQD^{PEI}s using colloidal solutions with different concentrations.

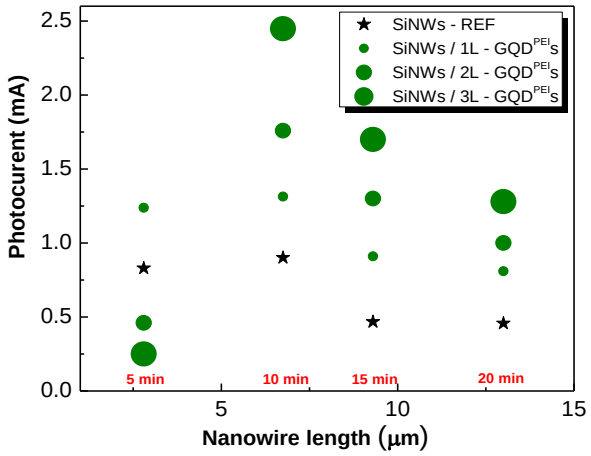

(a)

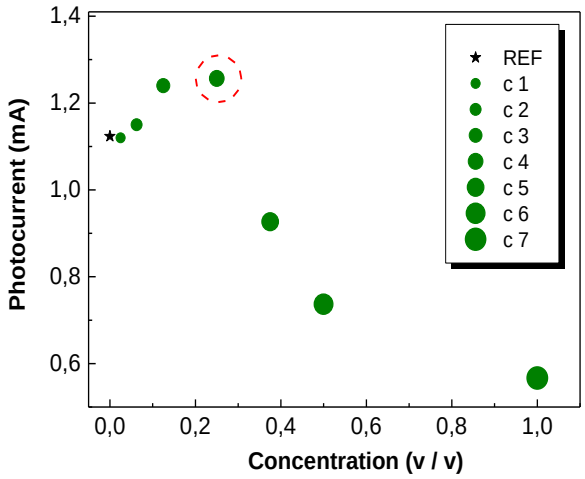

(b)

Figure S4 – Schottky heterojunction parameters.

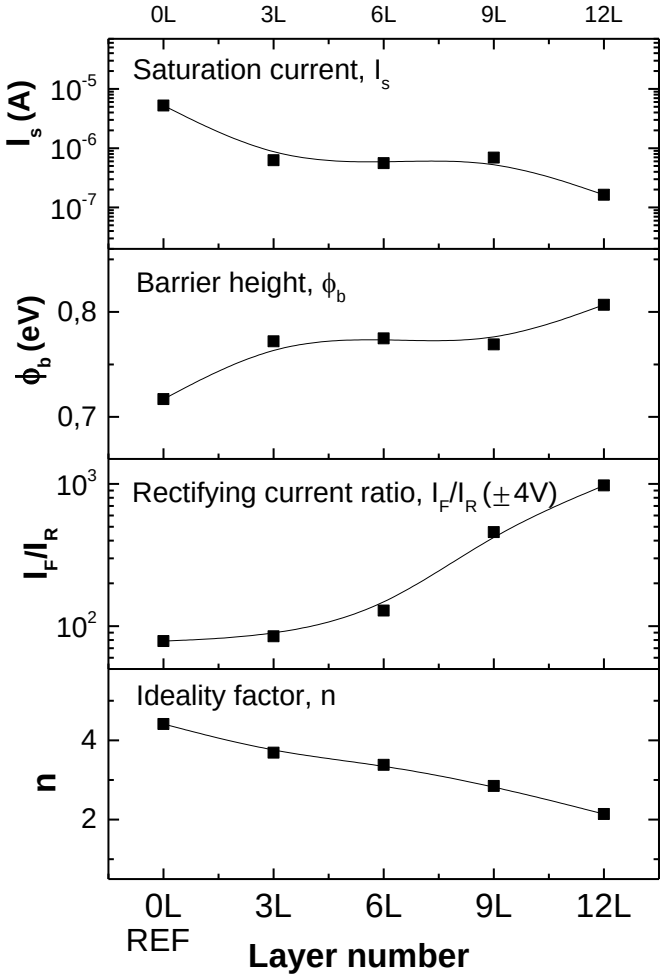

Figure S5 – Photo to dark current ratio as function of incident power at 1V (a) and 10 V (b) biases.

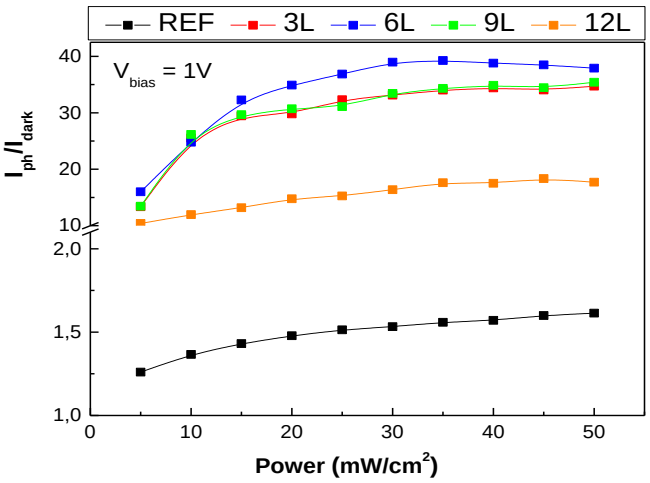

(a)

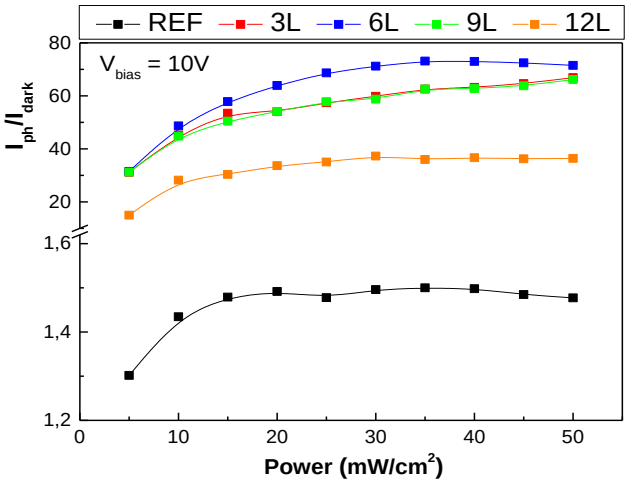

(b)

Figure S6 – Responsivity (a), detectivity (b) and external quantum efficiency (c) of the devices at 1V and 10 V bias, respectively. (d) EQE Enhancement of SiNWs based photodetectors integrated with GQD^{PEI} layer in comparison with reference SiNWs device at 1V and 10 V bias, respectively.

(a)

Responsivity

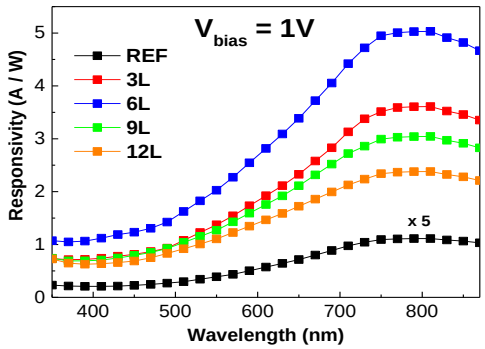

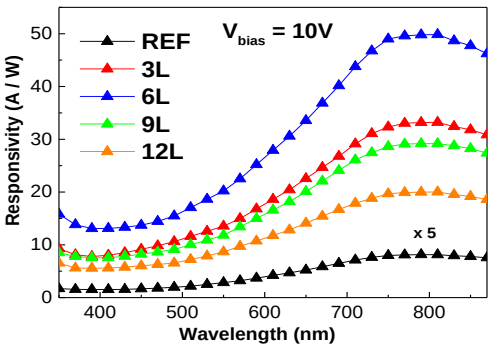

(b)

Detectivity

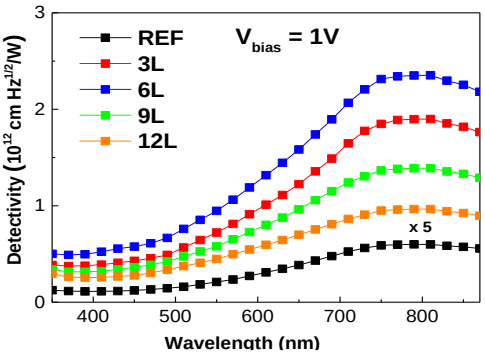

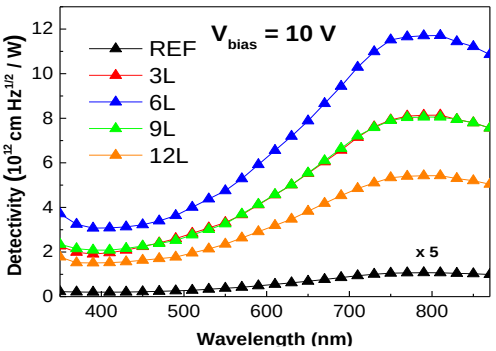

(c)

EQE

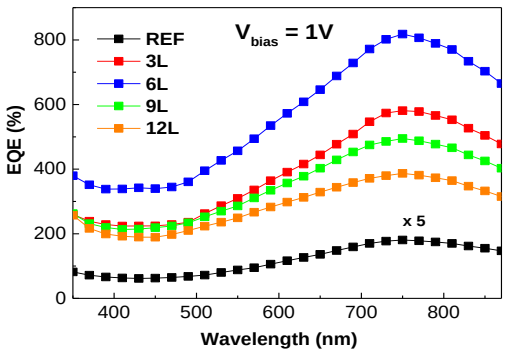

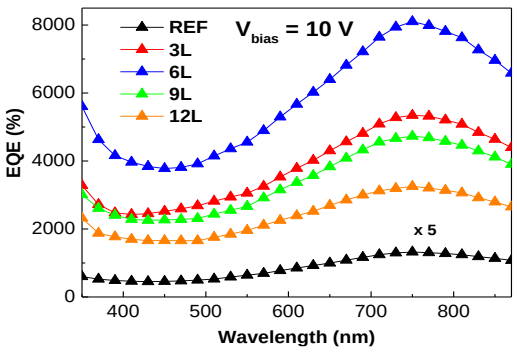

(d)

EQE enhancement

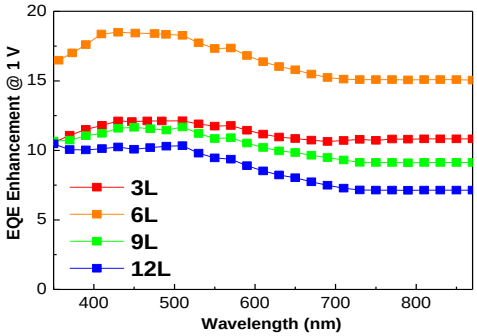

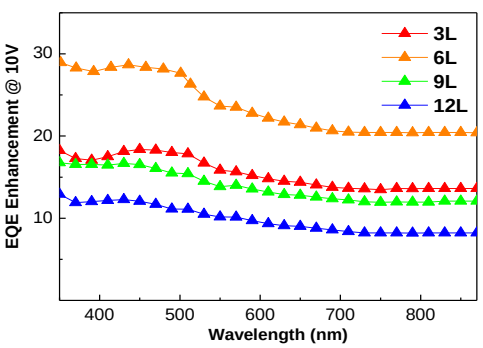

Figure S7 – Figure of merit for ITO/6L-GQD^{PEI}/p-SiNWs/Al heterostructure: (a) responsivity, (b) detectivity, (c) external quantum efficiency as function of the operation voltage, and (d) dynamic response measured with a bias of 4 V.

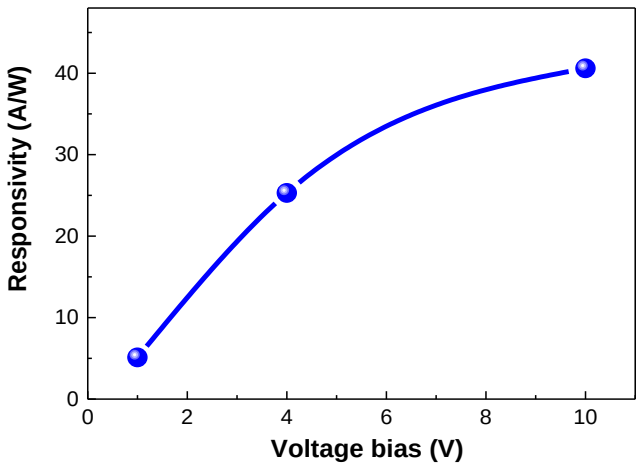

(a)

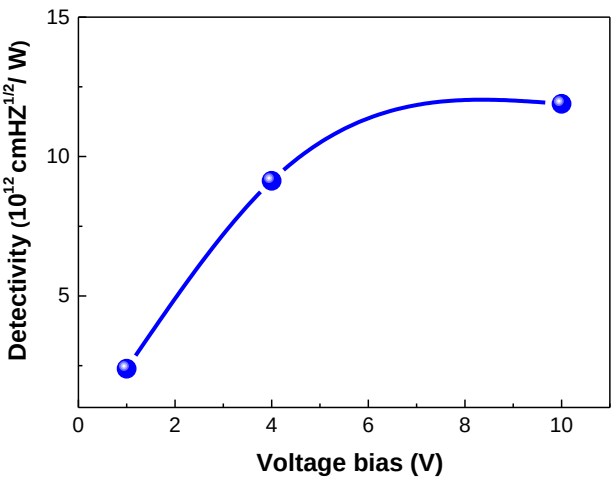

(b)

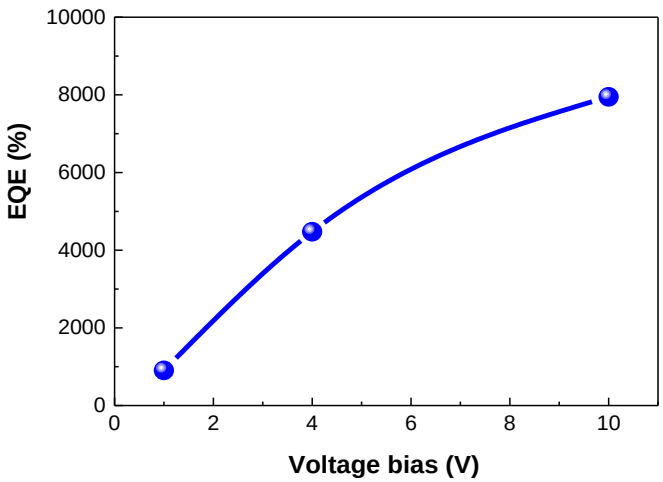

(c)

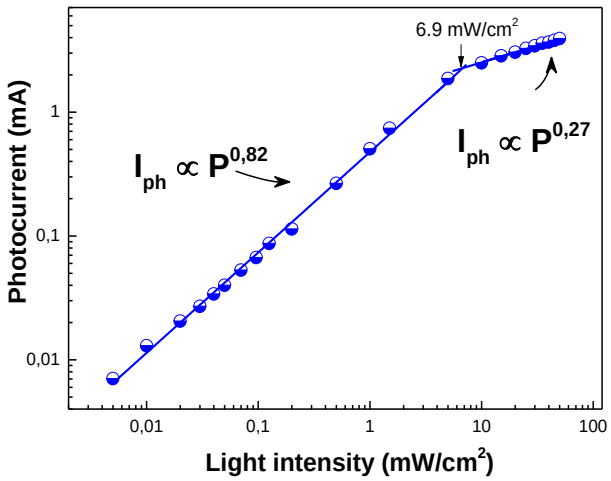

(d)

Table S1. Summary of the reported performances photodetector device with similar structures.

Device structure	Operating voltage (V)	Illumination conditions	Responsivity (A/W)	Detectivity ($cm \cdot Hz^{1/2}/W$)	EQE (%)	Rise/fall times	Ref.
6L-GQD^{PEI}/SiNWs	1	AM 1.5 G solar simulator (5 µW/cm^2 -100 mW/cm^2)	5	2.35 x 10^{12}	818	-	This work
	4		25.3	9 x 10^{12}	4200	78 / 73 ms	
	10		40.6	11.9 x 10^{12}	8150	-	
horizontally aligned SiNWs onto a substrate	1	808 nm laser (0.1 W/mm^2, 3Hz optical chopper)	-	-	-	10.96 / 19.26 ms	[1]
ITO/SiNWs	0.5	150W halogen lamp, pulsed 405 nm laser	0.55	-	70	4.3 / 10 µs	[2]
RGO/SiNWs	1	532 nm laser (218 mW)	0.33	-	-	10.6 / 6.7 s	[3]
		1064 nm laser (317 mW)	0.44	-	-	14.4 / 3.3 s	
		10.6 µm CO_2 laser	1.65	-	-	27.0 / 25.5 s	
		119 µm gas laser	0.62	-	-	21.4 / 23.3 s	
CdS/SiNWs	1	Xe lamp (100 mW/cm^2)	1.37	0.44 x 10^{12}	243	-	[4]
CdTe/SiNWs	2	AM 1.5 G solar simulator (85 mW/cm^2)	0.5	9 x 10^{12}	80	< 1 s	[5]
ZnO:N/SiNWs	5	500 W Hg (Xe) – arc lamp	0.98	-	-	-	[6]
TiO_2_NPs/SiNWs	1	He-Ne laser (632.8 nm, 0.95 mW)	0.801	2.44 x 10^{10}	157.01		[7]
PAA/SiNWs	1	He-Ne laser (632.8 nm, 0.95 mW)	0.604	2.23 x 10^{10}	-	-	[8]
CQDs/$CuAlO_2$	0.1	Xe lamp (100 mW/cm^2)	-	-	-	95 / 85 ms	[9]
CQD/ZnO_nanorods	2	365 nm UV light, 1 mW/cm^2	0.003	8.33 x 10^{12}		21 / 13 ms	[10]
CQD/SiNWs	0.1	600 nm pulsed light, 100 mW/cm^2	0.353	3.79 x 10^9		20 / 40 µs	[11]

Figure S8 - Variation of the capacitance with the applied voltage for (a) 0, (b) 3, (c) 6, (d) 9 and (e) 12 layers - GQD^{PEI}s/SiNWs based photodetector measured at 5 kHz, 10 kHz, 50 kHz, 100 kHz and 200 kHz applied frequencies.

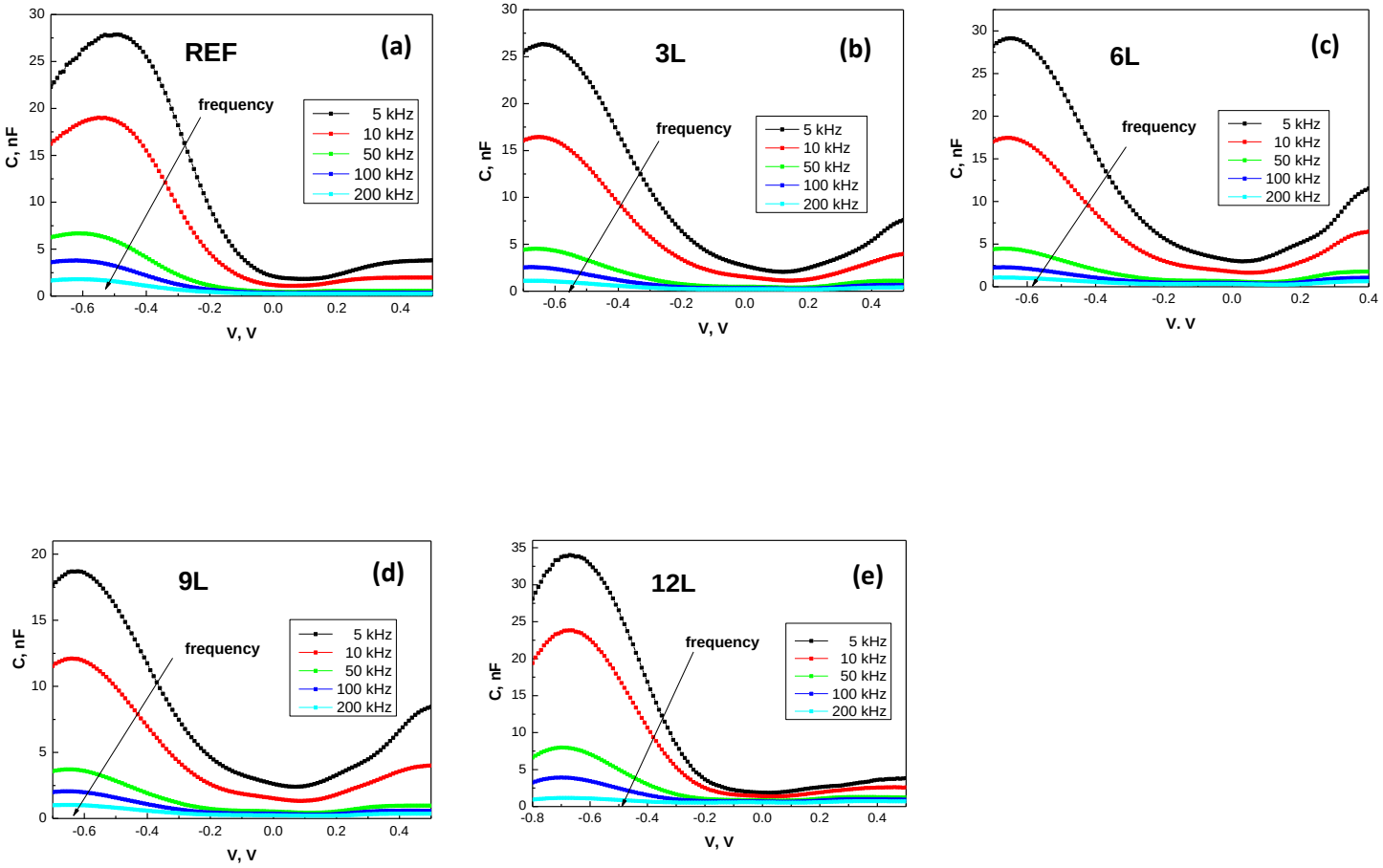

Figure S9 – Mott-Schottky analysis and the corresponding carrier concentration profiles as function of the applied voltage for (a) 0, (b) 3, (c) 6, (d) 9 and (e) 12 layers - GQD^{PEI}s/SiNWs based photodetector, highlighted for the depletion region.

The carrier concentration variation inside of the depletion region was analyzed using the equation:

$$N = \frac{-2}{q\varepsilon_0\varepsilon_r A^2}\left[\frac{d(C^{-2})}{dV}\right]^{-1} \quad (1)$$

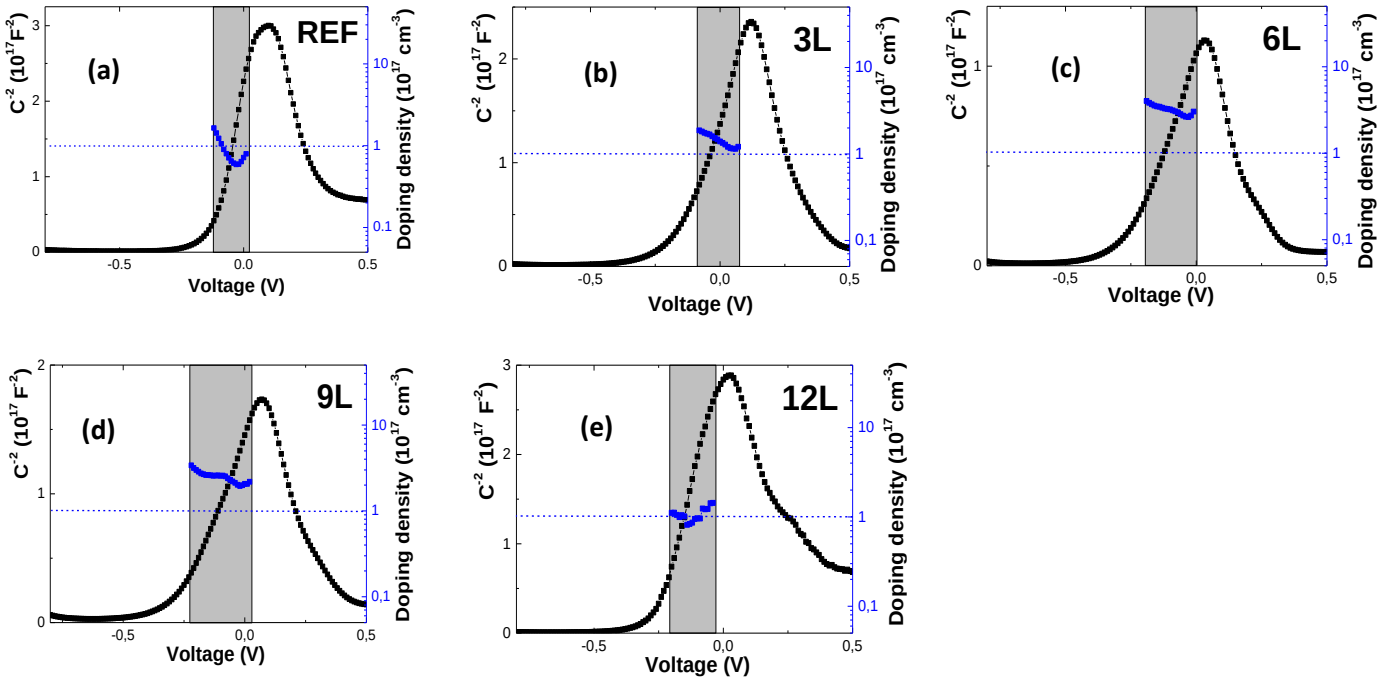

Figure S10 - Carrier concentration - N (a), and built-in voltage - V_{bi} (b) plots as function of frequency obtained from the fits of reverse-bias C^{-2} –V curves of the photodiodes at 300 K under dark conditions.

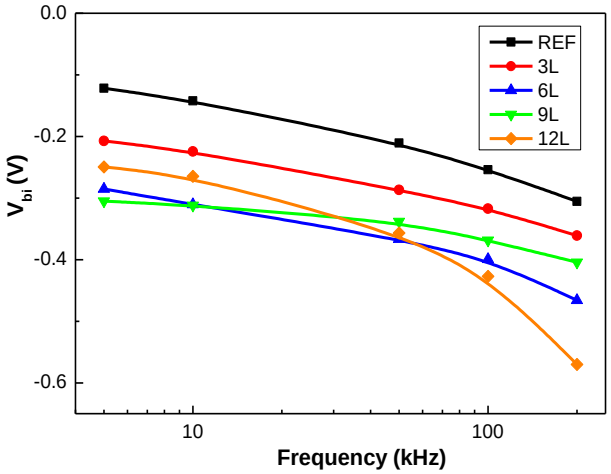

(a)

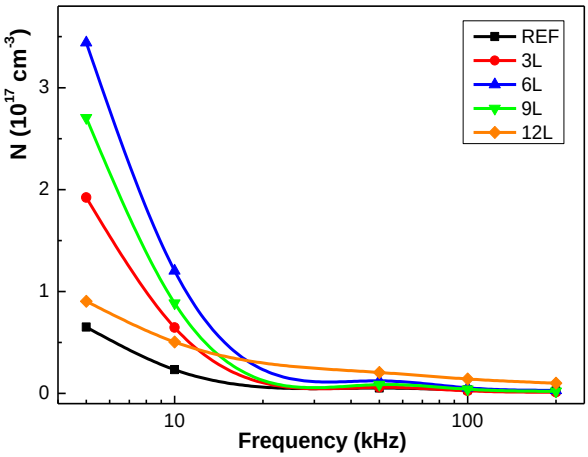

(b)

Figure S11 – Photoluminescence excitation (PLE) spectra at 580 nm emission peak, experimental data recorded for GQD^{PEI}s/SiNWs heterojunction and theoretical prediction of GQD^{PEI}s PLE behavior under SiNWs light trapping effect.

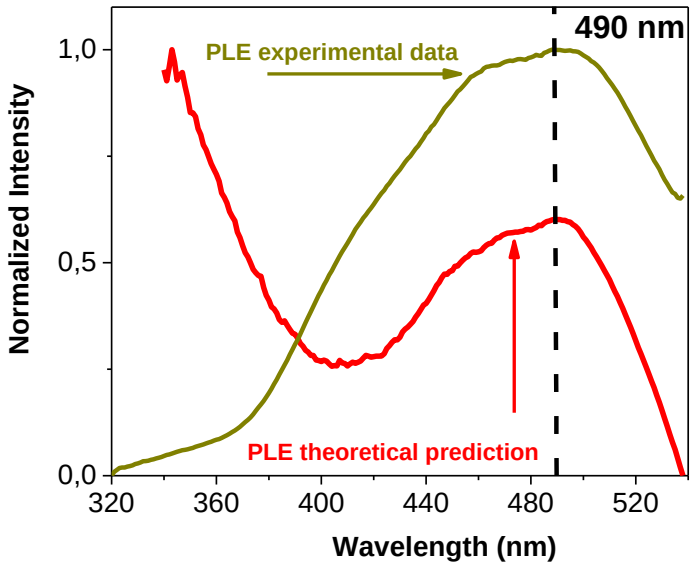

Figure S12 – Fluorescence decay profiles of solid-state GQD^{PEI}s measured at room temperature, deposited on planar and Si nanowires substrates, respectively.

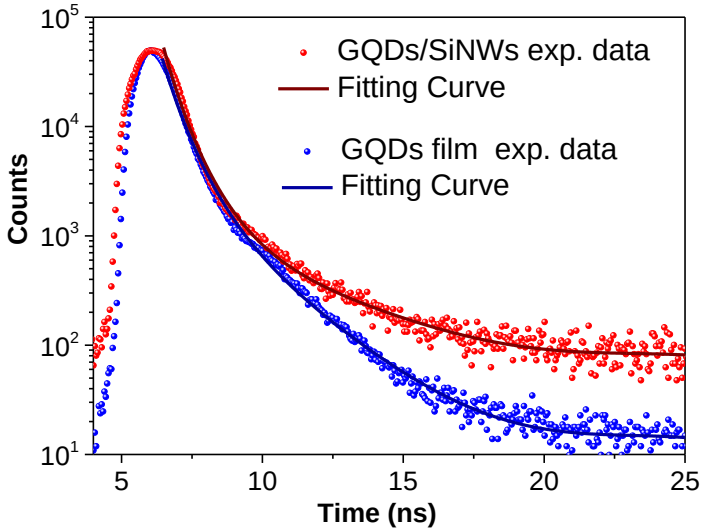

Table S2. Fluorescence decay times of GQD^{PEI}s films deposited on planar and Si nanowires substrates, respectively.

Sample	τ_1 [ns]	a_1[%]	τ_2 [ns]	a_2[%]	$< \tau >$ [ns]
GQDs film	0.51	45	1.84	55	0.83
GQDs on SiNWs substrate	0.46	67	1.93	33	0.61

Supporting Information References

[1] Zhang, D.; Cheng, G.; Wang, J.; Zhang, C.; Liu, Z.; Zuo, Y.; Zheng, J.; Xue, C.; Li, C.; Cheng, B.; Wang, Q. Horizontal Transfer of Aligned Si Nanowire Arrays and Their Photoconductive Performance. *Nanoscale Res. Lett.* **2014**, *9*, 661.

[2] Bae, J.; Kim, H.; Zhang, X. M.; Dang, C. H.; Zhang, Y.; Choi, Y. J.; Nurmikko, A.; Wang, Z. L. Si Nanowire Metal-Insulator-Semiconductor Photodetectors as Efficient Light Harvesters. *Nanotechnology* **2010**, *21*, 095502.

[3] Cao, Y.; Zhu, J.; Xu, J.; He, J.; Sun, J.-L.; Wang, Y.; Zhao, Z. Ultra-Broadband Photodetector for the Visible to Terahertz Range by Self-Assembling Reduced Graphene Oxide-Silicon Nanowire Array Heterojunctions. *Small* **2014** *10*, 2345–2351.

[4] Manna, S.; Das, S.; Mondal, S. P.; Singha, R.; Ray, S. K. High Efficiency Si/Cds Radial Nanowire Heterojunction Photodetectors Using Etched Si Nanowire Templates. *J. Phys. Chem. C* **2012**, *116*, 7126−7133.

[5] Akgul, F. A.; Akgul, G.; Gullu, H. H.; Unalan, H. E.; Turan, R. Enhanced Diode Performance in Cadmium Telluride–Silicon Nanowire Heterostructures, *J. Alloy. Compd.* **2015**, *644*, 131-139.

[6] Kang, H.; Park, J.; Choi, T.; Jung, H.; Lee, K. H.; Im, S.; Kim, H. n-ZnO:N/p-Si Nanowire Photodiode Prepared by Atomic Layer Deposition. *Appl. Phys. Lett.* **2012**, *100*, 041117.

[7] Rasool, K.; Rafiq, M. A.; Ahmad, M.; Imran, Z.; Hasan, M. M. TiO_2 Nanoparticles and Silicon Nanowires Hybrid Device: Role of Interface on Electrical, Dielectric, and Photodetection Properties. *Appl. Phys. Lett.* **2012**, *101*, 253104.

[8] Rasool, K.; Rafiq, M. A.; Ahmad M.; Imran, Z.; Batool, S. S.; Hasan, M. M. Photodetection and transport properties of surface capped silicon nanowires arrays with polyacrylic acid. *AIP Adv.* **2013**, *3*, 082111.

[9] Pan, J.; Sheng, Y.; Zhang, J.; Wei, J.; Huang, P.; Zhang, X.; Feng, B. The Photosensitivity of Carbon Quantum Dots/$CuAlO_2$ Films Composites. *Nanotechnol.* **2015**, *26*, 305201.

[10] Lee, S.-W.; Choi, K.-J.; Kang, B.-H.; Lee, J.-S.; Kim, S.-W.; Kwon, J.-B.; Gopalan, S.-A.; Bae, J.-H.; Kim, E.-S.; Kwon, D.-H.; Kang, S.-W. Low Dark Current and Improved Detectivity of Hybrid Ultraviolet Photodetector Based on Carbon-Quantum-Dots/Zinc-Oxide-Nanorod Composites. *Organic Electronics* **2017**, *39*, 250-257.

[11] Xie, C.; Nie, B.; Zeng, L.; Liang, F.-X.; Wang, M.-Z.; Luo, L.; Feng, M.; Yu, Y.; Wu, C.-Y.; Wu, Y.; Yu, S.-H. Core–Shell Heterojunction of Silicon Nanowire Arrays and Carbon Quantum Dots for Photovoltaic Devices and Self-Driven Photodetectors. *ACS Nano* **2014**, *8*, 4015-4022.